บทความวิจัย

NUMERICAL STUDY OF HEAT TRANSFER AND FLUID FLOW IN A CONFINED PLANE TURBULENT JET IMPINGEMENT USING NANOFLUIDS

Khomgris Chaiyo[1*]

[1]Department of Mechanical Engineering, Faculty of Engineering at Kamphaengsaen, Kasetsart University, Kamphaengsaen Campus, Nakhonpathom, 73140

[*]E-mail: khomgris.c@ku.th

Received: 2021-02-05

Revised: 2021-05-13

Accepted: 2021-06-08

ABSTRACT

This article presents a numerical investigation on heat transfer and fluid flow of a confined plane turbulent nanofluid jet impingement on an isothermal heated surface using a single-phase model. The finite volume method and standard k-ε turbulent model were used for the solution of resulting governing equations. Al_2O_3 nanoparticles dispersed in water with volumetric concentration of nanoparticles ranging between 0 and 4% were used as working fluid for simulating the heat transfer and fluid flow of nanofluid jet impingement. At inlet mean velocity profile was non-uniform. The influences of volumetric concentration of nanoparticles, aspect ratio and Reynolds number were examined and discussed in details. The results indicated that the volumetric concentration of nanoparticles, aspect ratio and Reynolds number enhanced heat transfer when considering in terms of the local and average Nusselt number, while the skin friction coefficient profile was slightly increased whereas increasing the volumetric concentration of nanoparticles.

Keywords: impinging jet, heat transfer enhancement, nanofluids

Introduction

Impinging jets provide an effective and flexible way to transfer energy or mass in industrial applications. The directed liquid or gaseous flow released against a surface can efficiently transfer large amounts of thermal energy or mass between the surface and the fluid. Heat transfer applications include cooling of stock material during material forming processes, heat treatment (Ferrari et al., 2003), cooling of electronic components, heating of optical surfaces for defogging, cooling of turbine

components, cooling of critical machinery structures, and many other industrial processes (Zuckerman et al., 2006).

Nanofluids are suspensions of very fine solid particles (nanoparticles) with length scales of 1–100 nm dispersed in base fluids, such as water, engine oil, and ethylene glycol (Choi et al., 1995). Due to the enhancement in thermal conductivity and heat transfer provided by nanofluids compared to classical heat transfer fluids. Nanofluids have become drastically significant for a wide range of engineering applications which require high heat dissipation rates such as heat exchangers (Venkitaraj et al., 2018) and cooling of electronic components which suffer from a high heat generation (Selvakumar et al., 2012). Integrating nanofluids with impinging jet is considered a promising technique that can overcome the challenges of heat removal (Abdelrehim et al., 2019).

Several researches have investigated numerically utilizing the single-phase model under a laminar flow regime using water-Al_2O_3 nanofluids. The hydrodynamic and thermal fields of a water-γAl_2O_3 nanofluid in a radial laminar flow cooling system were presented by Roy et al. (2004). The results indicated that considerable heat transfer enhancement is possible, even achieving a twofold increase in the case of a 10% nanoparticle volume fraction nanofluid. On the other hand, an increase in wall shear stress is also noticed with an increase in particle volume concentration.

A confined impinging slot jets working with pure water or water-Al_2O_3 based nanofluids was numerically presented. The flow is laminar and a constant uniform temperature is applied on the target surface. The single-phase model approach was adopted in order to describe the nanofluid behavior and different particle volume concentrations. The results demonstrated that the stagnation point the local heat transfer coefficient and Nusselt number values result to be the highest and they increase as particle concentrations and Reynolds numbers increase. The required pumping power ratio increases as particle concentration grows and it is at most 3.9 times greater than the values calculated in the case of pure water (Manca et al., 2016).

However, a few researches of turbulent impinging jet cooling using nanofluids have investigated numerically utilizing the single-phase model. A numerical analysis of a confined plane turbulent impinging jet with nanofluids was carried out to evaluate the thermal and fluid-dynamic performances and study the velocity and temperature fields. The base fluid is water and different volume concentrations of Al_2O_3 nanoparticles. The results demonstrated nanofluids produce an increase of fluid bulk temperature increasing concentrations, the highest values of the average Nusselt numbers increase as the nanoparticle concentrations and Reynolds numbers. Moreover, the velocity is set an uniform profile at inlet jet section (Manca et al., 2011).

The flow and heat transfer processes in a circular impinging jet of nanofluids water-Al_2O_3 were described by several different turbulence models and wall functions by Peng et al. (2014). The velocity and temperature fields were predicted by the single-phase model and the two-phase

model. The results indicated that two-phase model with the addition of nanoparticles significantly strengthens the momentum exchange between phases, promotes the uniformity of the temperature field, and, consequently, improves the overall heat transfer capacity, which cannot be predicted by the single-phase model.

Numerical investigations of turbulent flow field and heat transfer performance of water-Al_2O_3 nanofluid jet impingement were reported where jet impinged over a flat circular heated surface from a circular pipe of diameter. A single-phase mixture model and the control-volume approach were used. The uniform inlet velocity was applied at the jet inlet. The results indicated that the heat transfer increases with increasing values of the particle volumetric concentration while the flow field and turbulent kinetic energy distribution remain unchanged with the inclusion of nanoparticles (Allauddin et al., 2018).

Although a few researches are currently available on the numerical study of turbulent heat transfer and fluid flow of nanofluids impingement jet, there is no comprehensive study on at the inlet mean velocity profile that is non-uniform. The objective of this study is carried out to numerical evaluate the results of heat transfer and fluid flow obtained by the single-phase model in a confined plane turbulent jet impingement using nanofluids to cool the isothermal heated surface. The jet stream at inlet have an almost flat mean velocity profile that is non-uniform and specified according to Tsubokura et al. (2003). Furthermore, the influences of volumetric concentration of nanoparticles, aspect ratio and Reynolds number (Re) are investigated.

Methods

A. Problem description

The flow of the impinging jet is assumed to be steady, two-dimensional, turbulent, and incompressible as shown in Figure 1. The body forces are neglected and the fluid properties are assumed to be temperature independent. Brownian motion and thermophoretic diffusions of the nanoparticles do not have any significant effect on convection heat transfer for the percentage of nanoparticle concentration considered in this study. The length of the isothermal impingement surface to the width of the impinging jet was fixed at L/B=50, this isothermal impingement had a constant temperature of 310 K. The aspect ratios (H/B) were ranged from 4 to 8 to study the confining effect, and the flow was considered turbulent with varied from 10000 to 30000. The working fluid is water-Al_2O_3 nanofluids with the volumetric concentration of nanoparticles ϕ ranged from 0 to 4%.

B. Thermophysical properties of nanofluids

The numerical simulations were performed using water-Al_2O_3 nanofluids and the nanoparticle concentrations considered in the present analysis are as 0%, 1%, 2%, and 4%. The thermophysical properties of pure water and alumina are given in Table 1 (Rohsenow et al., 1998).

When the single-phase model was adopted in the present work as nanofluids with small nanoparticle volume fractions can be considered as Newtonian fluids for small temperature jumps (Mookherjee et al., 2020). The density and the specific heat of the nanofluids are evaluated using the formula developed for conventional solid–liquid mixtures as follow:

$$\rho_{nf} = (1 - \phi)\rho_{bf} + \phi\rho_{p} \quad (1)$$

$$(\rho C)_{nf} = (1 - \phi)(\rho C)_{bf}\rho_{bf} + \phi(\rho C)_{p} \quad (2)$$

where ϕ , ρ_{bf}, ρ_{p}, C_{bf} , and C_{p} are the volumetric concentration of nanoparticles, density of the base fluid, density of the nanoparticles, specific heat of the base fluid, and the specific heat of the nanoparticles, respectively. The viscosity and thermal conductivity of nanofluids are evaluated to follow Masoumi et al. (2009) & Chon et al. (2005) respectively .The thermophysical properties of the working fluid are summarized in Table 2 (Mookherjee 2020).

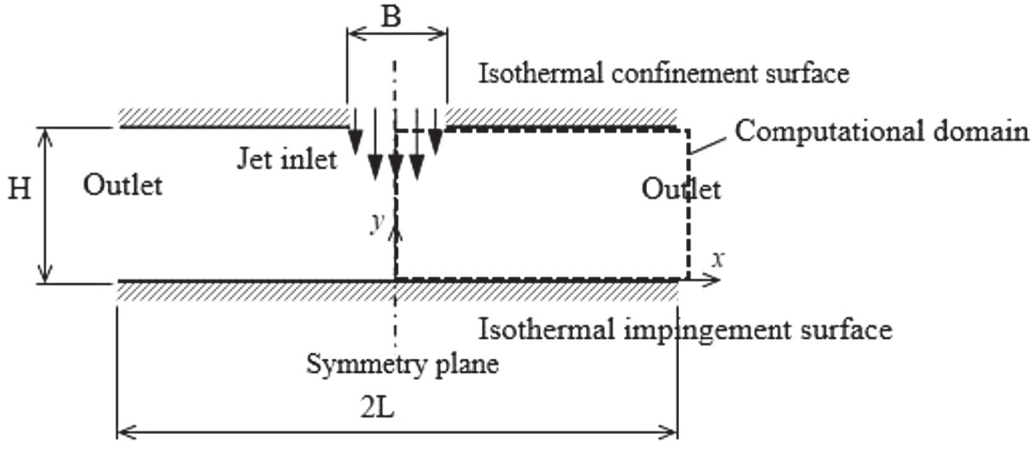

Figure 1 The two-dimensional confined impinging jet

C. Governing equations

The governing equations of the time-averaged formulation include the conservation equations of mass, momentum, and energy. In the present study, flows are assumed to be steady and incompressible, and the eddy viscosity concept is used to model the Reynolds stress (Launder et al., 1974). The continuity, momentum, and energy equations of the time-averaged equations can be written in the two-dimensional Cartesian coordinate system form as follows:

Continuity:

$$\frac{\partial}{\partial x}\left(\rho\bar{u}\right)+\frac{\partial}{\partial y}\left(\rho\bar{v}\right)=0 \tag{3}$$

x-momentum:

$$\frac{\partial}{\partial x}\left(\rho\overline{uu}\right)+\frac{\partial}{\partial y}\left(\rho\overline{uv}\right)=-\frac{\partial\bar{p}^{*}}{\partial x}+\frac{\partial}{\partial x}\left[\left(\mu+\mu_{t}\right)\frac{\partial\bar{u}}{\partial x}\right]+\frac{\partial}{\partial y}\left[\left(\mu+\mu_{t}\right)\frac{\partial\bar{u}}{\partial y}\right] \tag{4}$$

y-momentum:

$$\frac{\partial}{\partial x}\left(\rho\overline{uv}\right)+\frac{\partial}{\partial y}\left(\rho\overline{vv}\right)=-\frac{\partial\bar{p}^{*}}{\partial y}+\frac{\partial}{\partial x}\left[\left(\mu+\mu_{t}\right)\frac{\partial\bar{v}}{\partial x}\right]+\frac{\partial}{\partial y}\left[\left(\mu+\mu_{t}\right)\frac{\partial\bar{v}}{\partial y}\right] \tag{5}$$

Energy:

$$\frac{\partial}{\partial x}\left(\rho\bar{u}\bar{T}\right)+\frac{\partial}{\partial y}\left(\rho\bar{v}\bar{T}\right)=\frac{\partial}{\partial x}\left[\mu_{e}\frac{\partial\bar{T}}{\partial x}\right]+\frac{\partial}{\partial y}\left[\mu_{e}\frac{\partial\bar{T}}{\partial y}\right] \tag{6}$$

where $\bar{u}$, $\bar{v}$ are the mean velocities in the streamwise and crosswise directions respectively, $\bar{T}$ is the mean temperature, and ρ is the density. Besides, μ_t is the eddy viscosity (the turbulent viscosity) and the modified pressure, $\bar{p}^{*}$, is defined as:

$$\bar{p}^{*}=\bar{p}+\frac{2}{3}k \tag{7}$$

with $\bar{p}$ is the mean pressure, and k is the turbulence kinetic energy. The effective diffusion coefficient (μ_e) is defined as:

$$\mu_{e}=\left(\frac{\mu}{\mathrm{Pr}}+\frac{\mu_{t}}{\mathrm{Pr}_{t}}\right) \tag{8}$$

where Pr is the Prandtl number, and Pr_t is the turbulent Prandtl number, respectively.

E. The standard k-ε model

In the case of Reynolds Averaged Navier-Stokes (RANS) equation, a standard turbulence model such as the turbulence kinetic energy (k) and its dissipation rate (ε) are:

Turbulent kinetic energy:

$$\frac{\partial}{\partial x}\left(\rho\bar{u}k\right)+\frac{\partial}{\partial y}\left(\rho\bar{v}k\right)=\frac{\partial}{\partial x}\left[\left(\mu+\frac{\mu_{t}}{\sigma_{k}}\right)\frac{\partial k}{\partial x}\right]+\frac{\partial}{\partial y}\left[\left(\mu+\frac{\mu_{t}}{\sigma_{k}}\right)\frac{\partial k}{\partial y}\right]+P_{k}-\rho\varepsilon \tag{9}$$

Turbulent kinetic energy:

$$\frac{\partial}{\partial x}\left(\rho\bar{u}k\right)+\frac{\partial}{\partial y}\left(\rho\bar{v}k\right)=\frac{\partial}{\partial x}\left[\left(\mu+\frac{\mu_t}{\sigma_k}\right)\frac{\partial k}{\partial x}\right]+\frac{\partial}{\partial y}\left[\left(\mu+\frac{\mu_t}{\sigma_k}\right)\frac{\partial k}{\partial y}\right]+P_k-\rho\varepsilon \quad (9)$$

Dissipation rate:

$$\frac{\partial}{\partial x}\left(\rho\bar{u}\varepsilon\right)+\frac{\partial}{\partial y}\left(\rho\bar{v}\varepsilon\right)=\frac{\partial}{\partial x}\left[\left(\mu+\frac{\mu_t}{\sigma_\varepsilon}\right)\frac{\partial \varepsilon}{\partial x}\right]+\frac{\partial}{\partial y}\left[\left(\mu+\frac{\mu_t}{\sigma_\varepsilon}\right)\frac{\partial \varepsilon}{\partial y}\right]+C_{\varepsilon 1}P_k\frac{\varepsilon}{k}-C_{\varepsilon 2}\rho\frac{\varepsilon^2}{k} \quad (10)$$

The production of the turbulent kinetic energy, P_k, is formulated as:

$$P_k=\mu_t\left(\frac{\partial\bar{u}_i}{\partial x_j}+\frac{\partial\bar{u}_j}{\partial x_i}\right) \quad (11)$$

The production of the turbulent kinetic energy, P_k, is formulated as:

$$P_k=\mu_t\left(\frac{\partial\bar{u}_i}{\partial x_j}+\frac{\partial\bar{u}_j}{\partial x_i}\right) \quad (11)$$

The turbulent viscosity is defined as:

$$\mu_t=\rho C_\mu\frac{\varepsilon^2}{k} \quad (12)$$

The model constants are given by

$$C_\mu=0.09,\quad C_{\varepsilon 1}=1.44,\quad C_{\varepsilon 2}=1.92,\quad \sigma_k=1.0,\quad \sigma_\varepsilon=1.3$$

Since the laminar sublayer has effects on the flow near walls, the velocities, turbulent kinetic energy and its dissipation rates in this near wall regions may be evaluated by the wall function approaches (Launder 1974).

Table 1 Thermophysical properties of pure water and Al_2O_3 particles at T = 293 K used in the computations

Material	Density ρ (kg/m^3)	Heat capacity c (J/kg . K)	Viscosity μ (Pa . S)	Thermal conductivity λ (W/m . K)
Al_2O_3	3380	773	-	36
Water	998.2	4182	$993x10^{-6}$	0.597

Table 2 Thermophysical properties of working fluids

Volume fraction ϕ	Density ρ (kg/m^3)	Heat capacity c (J/kg . K)	Viscosity μ (Pa . S)	Thermal conductivity λ (W/m . K)
0%	998.2	4182	$993x10^{-6}$	0.597
1%	1027.018	4053.210	$1097.05x10^{-6}$	0.617
2%	1055.836	3931.451	$1154.756x10^{-6}$	0.631
4%	1113.472	3706.841	$1375.910x10^{-6}$	0.655

D. Numerical solution procedure

The computations have been performed with the in-house developed computational code. The governing equations and the transport equation of above turbulence models were solved using the finite volume method (Patankar, 1980). This scheme solves discretized versions of all equations with non-uniform staggered grids. The principle of mass-flux continuity is improved indirectly via the solution of pressure-correction equations according to SIMPLE algorithm (Patankar 1980). The convergence is judged by monitoring the magnitude of the absolute residual sources of mass, momentum and energy, normalized by the respective inlet fluxes. The solution is taken as having converged when all above residuals fell below 0.0001%.

The geometry of two-dimensional plane impinging jet consists of the jet stream, impinging and confinement wall; therefore as shown in Figure 1, computational boundaries involved are inlet, outlet, axis of symmetry and solid walls (isothermal impingement and confinement surfaces).

First at the inlet, the jet temperature $\overline{T}_j$ is given at 300 K. The jet stream having an almost flat mean velocity profile ($\overline{v}_{in}$) was specified according to Tsubokura (2003) as:

$$\overline{v}_{in} = \overline{v}_0 \left[1 - (2x/B)^{14} \right] \tag{13}$$

where B is jet width and $\overline{v}_0$ is the mean centerline velocity. The Reynolds number (Re) is calculated as:

$$\mathrm{Re} = \frac{\rho \overline{v}_0 B}{\mu} \tag{14}$$

Next, the outlet boundary is placed at x=50B which is sufficiently far away from the main region of interesting. At this boundary streamwise gradients of all variables are set to zero. Then along the axis of symmetry, the normal velocity component and the normal gradients of other variables are set to zero.

Finally, at solid walls including impingement and confinement surface, the standard wall function approach is used to bridge the viscous sublayer at the duct wall which is based on standard k-ε model consideration. Also the walls are considered isothermal, the impingement surface T_w at 310 K and the confinement surface at 300 K, respectively. The Nusselt number (Nu) is defined as:

$$\mathrm{Nu} = \frac{-\left(\partial \overline{T} / \partial y\right)_w B}{\overline{T}_w - \overline{T}_j} \tag{15}$$

Before proceeding to the discussion of the predicted results, it will be beneficial to focus first on the effect of the grid density on the solution. Figure 2 shows the computational grid at distance x/B=50 and y/B=6, the grid clustering are applied near the impingement surface and the confinement surface. The grid-independency of the solutions are examined using three different grid sizes consisting of 12464 (82x152), 25944 (92x282) and 30804 (102x302) on the model H/B=6 at Re=20000 with water as working fluid. The results on the intermediate grid 92x282 can be considered as the grid-independent results because the refinement from the grid 92x282 to the grid 102x302 produces averaged too small Nusselt number difference as shown in Figure 3.

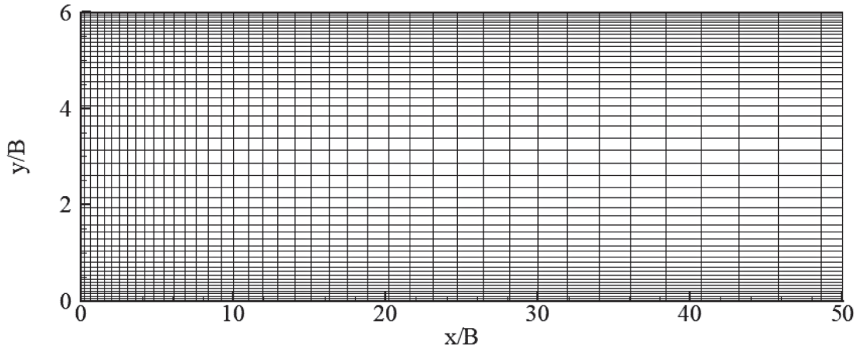

Figure 2 Sample of computational grid

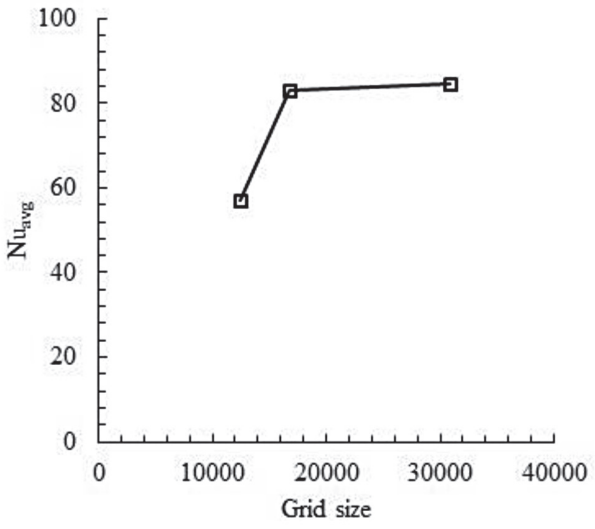

Figure 3 Grid independence analysis in the case of H/B=6 and Re=20000 using water as working fluid

Results and Discussions

The numerical results of a two-dimensional turbulent confined jet of Al2O3-water-based nanofluids impinging on a stationary isothermal wall are investigated. Including the influence of volumetric concentration of nanoparticles, aspect ratio and Reynolds number are presented.

A. Numerical validation

In order to verify the developed computational code, the simulation results including the Nusselt number and the skin friction coefficient along the impingement plate for H/B=9.2 and Re=20000 are compared with the experimental data (Ashforth-Frost et al., 1997) and previous numerical data (Kubacki et al., 2010). The present numerical results are in good agreement with the experimental data and also the previous numerical data as shown in Figures 4.

B. Influence of volumetric concentration of nanoparticles

The numerical results of heat transfer and fluid flow are investigated at the different volumetric concentrations of nanoparticles values as ϕ = 0%, 1%, 2%, and 4% for H/B=6 and Re=20000. Figure 5 illustrates streamlines in case of various volumetric concentrations of nanoparticles values for H/B=6 and Re=20000. The development of a vortex is generated by the impinging jet because of jet entrainment, confining effects, and isothermal confinement surface. It is seen that a vortex is generated below the jet. The main jet stream impinges on the target isothermal heated impingement surface, gets deflected, and then flows downstream in a meandering path in between the recirculation and the impingement surface toward the outlet. Similar streamline trends are observed all volumetric concentration of nanoparticles.

Figure 6 shows temperature distributions in case of various the volumetric concentration of nanoparticles for H/B=6 and Re=20000. The temperature profiles are increased with respect to the increase of volumetric concentration of nanoparticles because of improving thermal conductivity of nanofluids.

Figure 7(a) shows the Nulsselt number (Nu) distribution along the impingement surface for H/B=6 and Re=20000 at various volumetric concentration of nanoparticles. It is observed that the increased volumetric concentration of nanoparticles, the Nu is increased due to the increase of the thermal conductivity. Furthermore, the averaged Nulsselt number (Nuavg) distribution along the impingement surface is 83.06, 83.59, 83.57 and 84.75 for ϕ = 0%, 1%, 2% and 4%, respectively. However, the skin fiction coefficient along the impinging surface is slightly different due to the small effect of nanoparticle on the velocity field as shown in Figure 7(b). Additionally, it is clear on the averaged skin friction coefficient along the impingement plate is 0.004644, 0.004645, 0.004645 and 0.004645 at different volumetric concentrations ϕ = 0%, 1%, 2% and 4%, respectively.

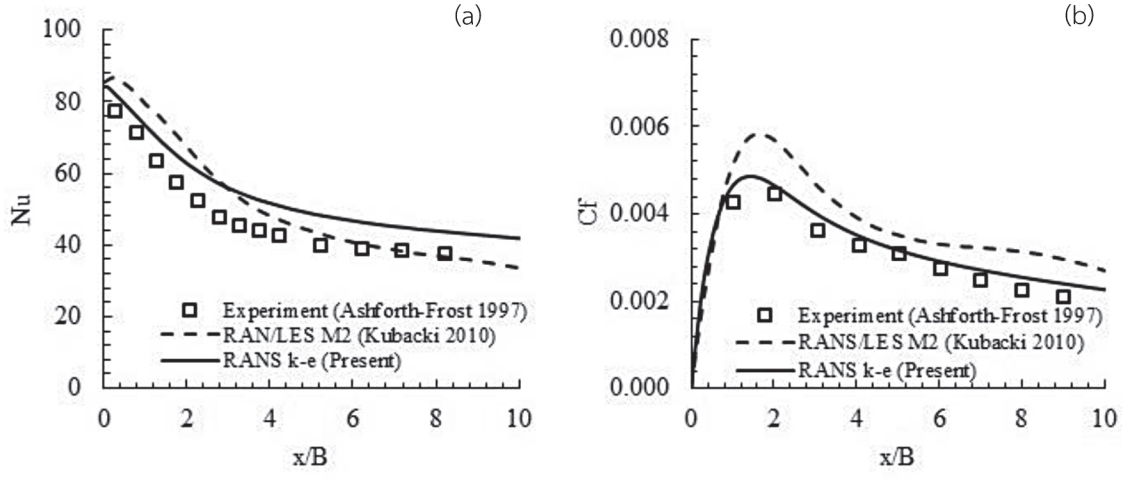

Figure 4 Comparison of present results with previous experimental and numerical data for H/B=9.2 and Re=20000 (a) The Nulsselt number distribution (b) The skin friction coefficient distribution

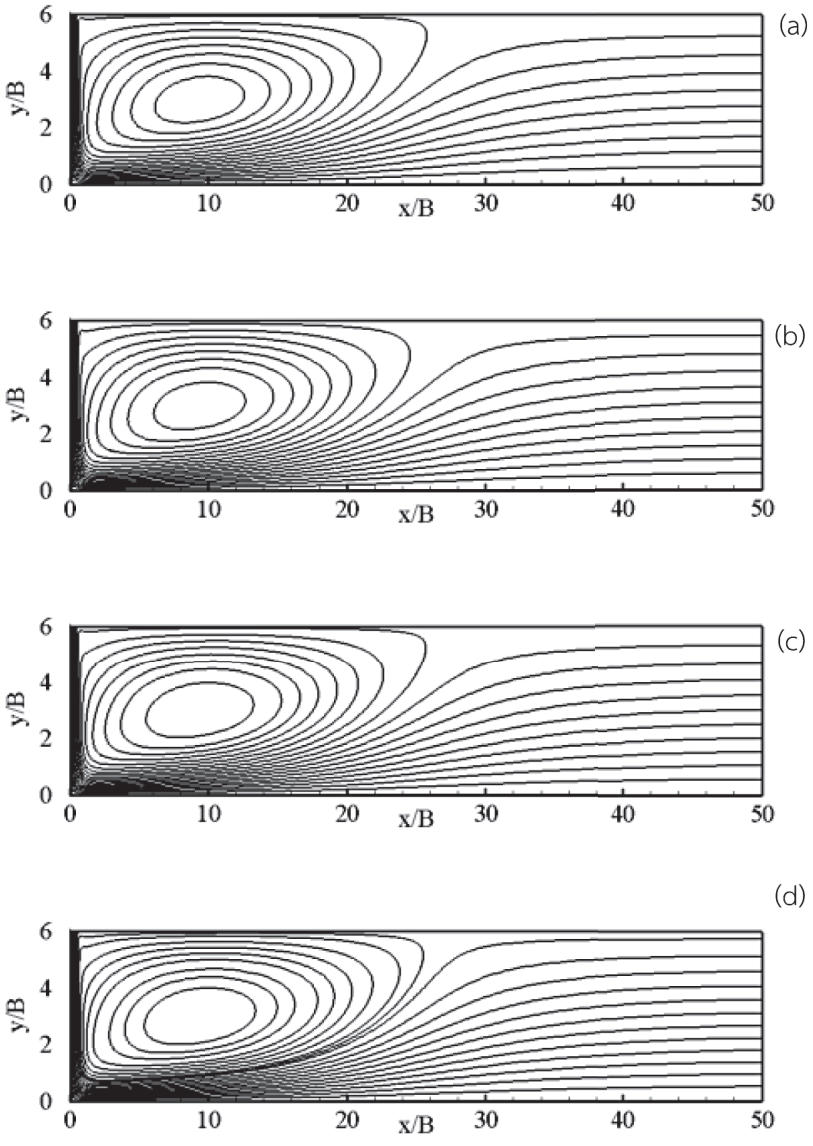

Figure 5 The streamlines at different volumetric concentrations of nanoparticles values for H/B=6 and Re=20000 (a) ϕ = 0%, (b) ϕ = 1%, (c) ϕ = 2%, (d) ϕ = 4%,

C. Influence of aspect ratio

The Nu distribution along the impingement surface for different aspect ratios H/B and volumetric concentration of nanoparticles ϕ=0% and 4% at Re=20000 as shown in Figure 8(a). Nu is the maximum value at the stagnation point and then it is exponentially decreased along the surface. This is because the increase of the thickness of thermal boundary layer and the decrease of the local velocity due to velocity boundary layer. Figure 8(b) shows the averaged Nu along the impingement surface at different aspect ratios for the volumetric concentration of nanoparticles

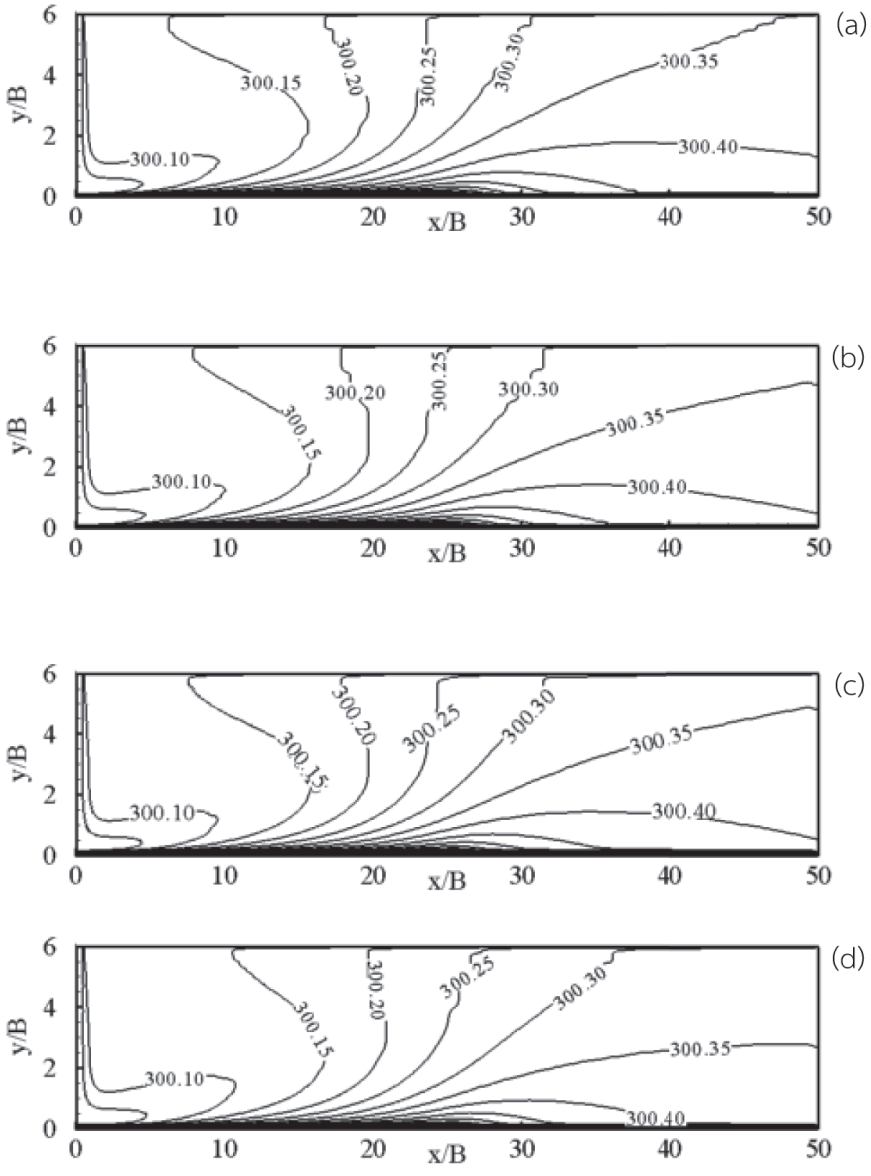

Figure 6 The temperature field at different volumetric concentration of nanoparticles values for H/B=6 and Re=20000 (a) ϕ=0%, (b) ϕ=1%, (c) ϕ=2%, (d) ϕ=4%,

ϕ=0% and 4% at Re=20000. The Nu_{avg} is risen by increasing H/B and also the maximum Nu_{avg} is found at largest H/B=8

D. Influence of Reynolds number

For different Re and the volumetric concentrations of nanoparticles ϕ=0% and 4% at H/B=6 are investigated. The influence of Re on the heat transfer can also be clarified in terms of Nu and Nu_{avg}. as shown in Figures 9(a) and 9(b), respectively. Increasing Re leads to increase in the heat transfer due to the increase of the temperature gradient at the isothermal impingement surface

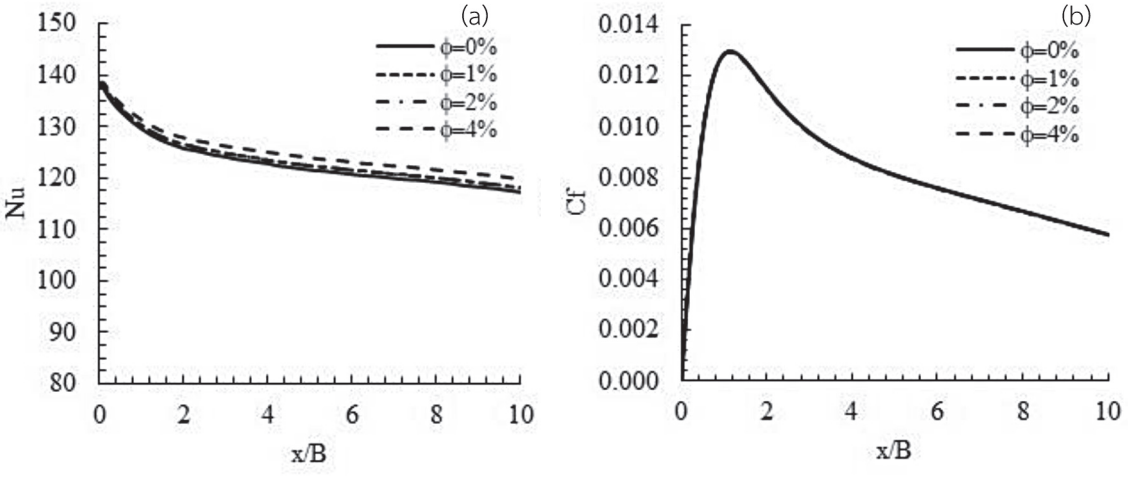

Figure 7 The results at different volumetric concentration of nanoparticles values for H/B=6 and Re=20000 (a) Nulsselt number distribution (b) The skin friction coefficient distribution

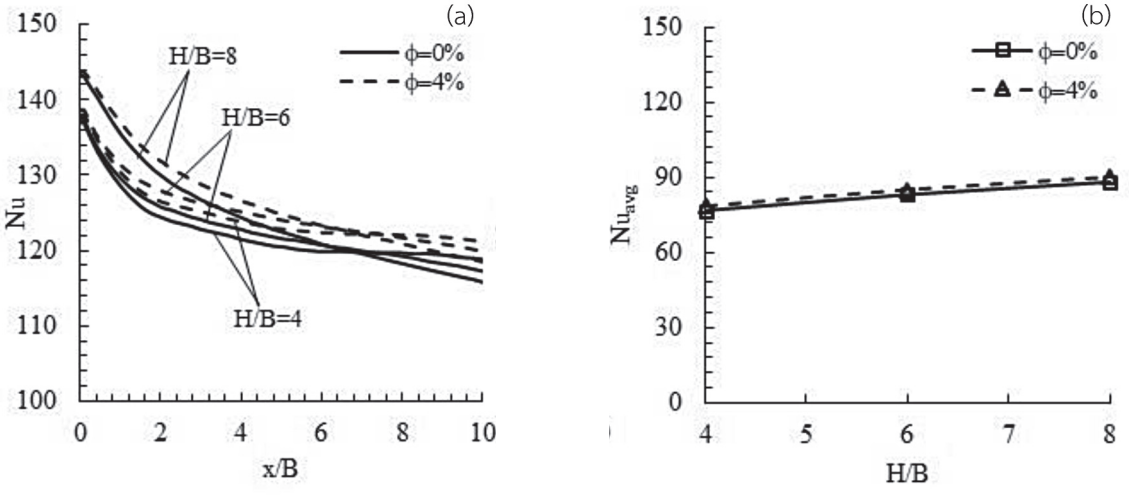

Figure 8 The Nulsselt number for various aspect ratios H/B at Re=20000 (a) Nu distribution along the impingement surface (b) the averaged Nu profile

Conclusions

The turbulent heat transfer and fluid flow of nanofluids in a confined plane jet impingement were numerically investigated using the single-phase and the standard k-ε model in the simulation of jet impingement flow was evaluated against previous experimental and numerical data that was found to produce good predictions of the local Nusselt number and the skin friction coefficient distribution along the impingement surface. The influences of volumetric concentration of nanoparticles, aspect ratio and Reynolds number are examined in details. Major findings can be summarized as follows:

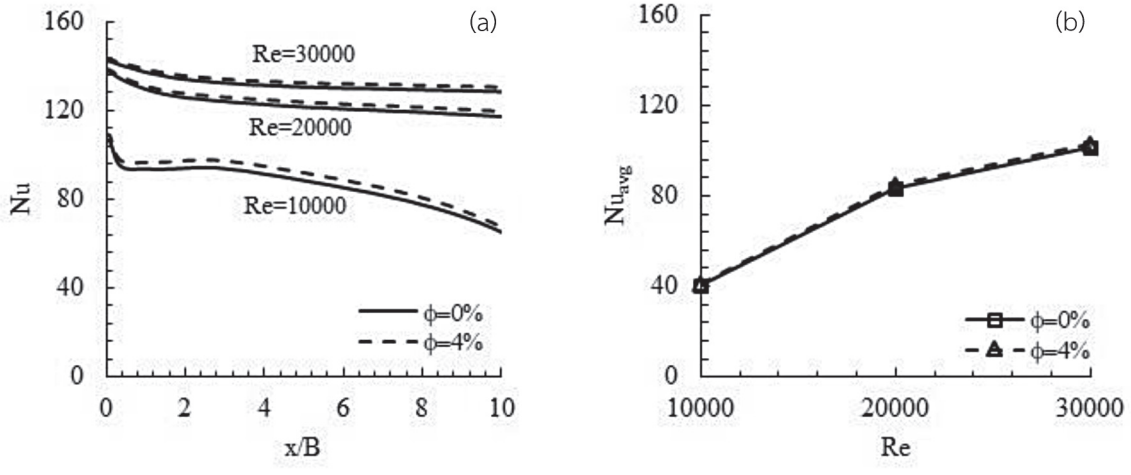

Figure 9 The Nulsselt number for various Re numbers at H/B=6 (a) Nu distribution along the impingement surface (b) the averaged Nu profile

(1) The volumetric concentration of nanoparticles ranging from 0 to 4% increase the heat transfer in terms of the local and average Nusselt number, while the skin friction coefficient profile is slightly increased whereas increasing the volumetric concentration of nanoparticles.

(2) Aspect ratio ranges from 4 to 8 similar to the flow Reynolds number varied from 10000 to 30000 enhance the heat transfer coefficient of nanofluids

Acknowledgement

The author gratefully acknowledge the Faculty of Engineering at Kamphaengsaen, Kasetsart University, Kamphaengsaen Campus, Nakhonpathom for supporting this research.

References

Abdelrehim, O., Khater, A, Mohamad, A.A., & Radwan, A. (2019). Two-phase simulation of nanofluid in a confined single impinging jet. **Case Studies in Thermal Engineering, 14**, 100423.

Allauddin, U., Mahrukh, M., Rehman, N.U., Haque, M. E., & Uddin, N. (2018). Numerical investigation of heat transfer by an impinging jet using alumina–water nanofluid. **Numerical Heat Transfer A, 74**(8), 1486-1502.

Ashforth-Frost, S., Jambunathan, K., & Whitney, C.F. (1997). Velocity and turbulence characteristics of a semiconfined orthogonally impinging slot jet. **Experimental Thermal and Fluid Science, 14**, 60–67.

Choi, S.U.S., & Eastman, J.A. (1995). Enhancing thermal conductivity of fluids with nanoparticles. **ASME International Mechanical Engineering Congress and Exposition, 66**, 99–105.

Chon, C.H., Kihm, K.D., Lee, S.P., & Choi, S.U. (2005). Empirical correlation finding the role of temperature and particle size for nanofluid (Al_2O_3) thermal conductivity enhancement. **Applied Physics Letters, 87**, 153107-3.

Ferrari, J.,Lior, N., & Slycke, J. (2003). An evaluation of gas quenching of steel rings by multiple-jet impingement. **Journal of Materials Processing Technology, 136**, 190–201.

Kubacki, S., & E. Dick, E. (2010). Simulation of plane impinging jets with k–ε based hybrid RANS/LES models. **International Journal of Heat and Fluid Flow, 31,** 862–878.

Launder, B.E., & Spalding, D.B. (1974). The numerical computation of turbulent flows. **Computer Methods in Applied Mechanics and Engineering, 3,** 269-289.

Manca, O., Mesolella, P., Nardini, S., & Ricci, D. (2011). Numerical study of a confined slot impinging jet with nanofluids. **Nanoscale Research Letters, 6:**188.

Manca, O., Ricci, D., Nardini, S., & Lorenzo, G.D. (2016). Thermal and fluid dynamic behaviors of confined laminar impinging slot jets with nanofluids. **International Communications in Heat and Mass Transfer, 70,** 15–26.

Masoumi, N., Sohrabi, N., & Behzadmehr, A. (2009). A new model for calculating the effective viscosity of nanofluids. **Journal of Physics D: Applied Physics, 42,** 0550-501.

Mookherjee, O., Pramanik, S., & Kar, U.K. (2020). Numerical investigation of a confined laminar jet impingement cooling of heat sources using nanofluids. **ASME Journal of Heat Transfer, 142**(8), 082301.

Patankar, S.V. (1980). **Numerical Heat Transfer and Fluid Flow.** New York: Hemisphere Publishing Corporation.

Peng, W., Jizu, L., Minli, B., Yuyan, W., & Chengzhi, H. (2014). A numerical investigation of impinging jet cooling with nanofluids. **Nanoscale and Microscale Thermophysical Engineering, 18,** 329–353.

Rohsenow, W.M., Hartnett, J.P., & Cho, Y.I. (1998). Handbook of Heat Transfer. 3rd Edition. New York: McGraw-Hill.

Roy, G., Nguyen, C.T., & Lajoie, P.R. (2004). Numerical investigation of laminar flow and heat transfer in a radial flow cooling system with the use of nanofluids. **Superlattices and Microstructures, 35,** 497–511.

Selvakumar, P., & Suresh, S. (2012). Convective performance of CuO/water nanofluid in an electronic heat sink. **Experimental Thermal and Fluid Science, 40,** 57–63.

Tsubokura, M., Kobayashi, T., Taniguchi, N., & Jones, W.P. (2003) A numerical study on the eddy structures of impinging jets exited at the inlet. **International Journal of Heat and Fluid Flow, 24,** 500–511.

Venkitaraj, K.P., Suresh S., Alwin Mathew, T., Bibin B.S., & Abraham, J. (2018). An experimental investigation on heat transfer enhancement in the laminar flow of water/TiO2 nanofluid through a tube heat exchanger fitted with modified butterfly inserts. **Heat and Mass Transfer, 54,** 813–829.

Zuckerman, N., & Lior, N. (2006). Jet impingement heat transfer: physics, correlations, and numerical modeling. **Advances in Heat Transfer, 39,** 565–631.